



1 A New View on Risk of Typhoon Occurrence in the Western 2 North Pacific

3 Kelvin. S. Ng¹, Gregor. C. Leckebusch¹

4 ¹School of Geography, Earth and Environmental Sciences, University of Birmingham, Birmingham, UK

5 *Correspondence to:* Kelvin S. Ng (k.s.ng@bham.ac.uk)

6

7 **Abstract.** To study high impact tropical cyclone (TC) is of crucial importance due to its extraordinary destruction
8 potential that leads to major losses in many coastal areas in the Western North Pacific (WNP). Nevertheless,
9 because of the rarity of high-impact TCs, it is difficult to construct a robust risk assessment based on the historical
10 best track records. This paper aims to address this issue by introducing a computationally simple and efficient
11 approach, using data from the THORPEX Interactive Grand Global Ensemble (TIGGE) archive with the
12 application of impact-oriented tracking algorithm, to build a physically consistent high impact typhoon event set
13 with non-realised TC events – data equivalent to more than 10,000 years of TC events. The temporal and spatial
14 characteristics of the new event set is consistent to the historical TC climatology in the WNP. It is shown that this
15 TC event set contains ~100 and ~77 times more Very Severe Typhoons and Violent Typhoons than the historical
16 records, respectively. Furthermore, this approach can be used to improve the return period estimation of TC-
17 associated extreme wind. Consequently, a robust extreme TC hazard risk assessment, reflective of the current
18 long-term climate variability phase, can be achieved using this approach.

19 1 Introduction

20 Increasing frequency and intensity of extreme meteorological events in the recent decades (IPCC, 2012) and
21 increasing number of human population and assets located in risk-prone regions (Desai et al., 2015) lead to an
22 increase of risk and loss potential to human and economic from natural disasters, for example tropical cyclones.
23 In the period of 1st January and 18th October 2018, typhoon-related total direct economic losses in Western North
24 Pacific (WNP) is up to 67.1 billion RMB (WMO, 2018). While natural disaster has impact to all stakeholder of
25 the society, governments are crucial in disaster risk reduction (DRR) because of their ability to implement
26 necessary DRR-related policy and ability to allocate resources to appropriate parties (Shi, 2012). Governments
27 have various options for DRR investments, for example, post-disaster relief and risk financing. Using cost-benefit
28 analysis for a case study of typhoon disasters in China, Ye et al. (2016) showed insurance premium subsidies has
29 the highest benefit-cost ratio. This is because premium subsidies increases penetration rate of an insurance
30 program, i.e. more protection is offered by the private sector and the risk is transferred to the private sector
31 (Glauber, 2004). Thus, development and application of effective financial instruments for risk transfer is
32 important.

33 Other than classical (re-)insurance solutions, parametric insurance solutions have been developed for test
34 cases in areas of corn yield (Sun et al., 2014) and life stock (Ye et al., 2017) for Southeast Asia and China in



35 recent years. Swiss Reinsurance Company Ltd. (SwissRe) insured several municipal governments in Guangdong
36 Province, China, through parametric insurance solution (Lemcke, 2017). Parametric insurance requires no
37 physical damage assessment after an event. As soon as a certain threshold (i.e. trigger point) is exceeded, the
38 insured party receives the agreed compensation from the insurer. Thus it has low administrative cost and quick
39 disbursement. However, it is a challenge to determine a robust trigger point. It is because it would require a
40 reliable typhoon risk assessment for the region of interest. A current common approach is to generate a large
41 typhoon event set (e.g. equivalent to 7,000 years of real world data) based on historical track data using stochastic
42 approach (e.g. Vickery et al., 2000; Emanuel, 2006; Emanuel et al., 2006; Rumpf et al., 2007, 2009). There are
43 two potential downsides with the stochastic approach: (i) such typhoon event set would be biased toward the past
44 events, and the frequency-intensity distribution of the event set might not be the same as the underlying frequency-
45 intensity distribution; (ii) the storms in the typhoon event set might not be physically consistent. Consequently,
46 the trigger point derived from the common approach may not be optimal. This means insurees could be either
47 over- or under-compensated by the insurer.

48 A method to increase number of extreme weather events is to make use of ensemble prediction system
49 (EPS). Osinski et al. (2016) used European Centre for Medium-Range Weather Forecasts (ECMWF) EPS to build
50 an event set of European windstorms. Osinski et al. (2016) pointed out there are two types of storm events
51 produced by EPS: (i) modified EPS storm (MEPS), and (ii) pure EPS storm (PEPS). MEPSs are storms with
52 modifications in the EPS which have real-world counterpart. PEPSs are storms in the EPS which have no real-
53 world counterpart, i.e. unrealised. PEPSs are independent events and the number of PEPSs increases as the lead
54 time increase until the model has no memory of the initial conditions. Thus one can form an event set of extreme
55 weather event by using TC related PEPSs. Osinski et al. (2016) demonstrated that reliable statistics of storms
56 under the observed climate conditions can be produced based on EPS forecasts.

57 Building upon the results of Osinski et al. (2016), a new approach to construct a large data volume,
58 physically consistent TC event set is presented in this study. This event set is constructed by applying an impact-
59 oriented windstorm tracking algorithm (WiTRACK; e.g. Leckebusch et al. 2008) to a multi-model global
60 operational ensemble forecast data archive, The THORPEX Interactive Grand Global Ensemble (TIGGE)
61 (Bougeault et al., 2010; Swinbank et al., 2015). The data volume of TIGGE is about 40,000 to 50,000 years. The
62 event set consists of all non-realised TC events which were forecasted by EPS of different centres, this event set
63 is referred to as the TIGGE PEPS (TPEPS) event set. In this study, we show the TPEPS event set has much higher
64 information content: more TC events and more extremely high impact TC events. The TPEPS event set can be
65 used to produce a robust TC risk assessment and to determine a robust trigger point for parametric typhoon
66 insurance.

67 In this paper, we first present a computationally simple, inexpensive and efficient method to construct a
68 physically consistent, high information content TC event set using only the 6-hourly surface wind speed field of
69 EPS forecast model outputs. Then we analyse the characteristics of the TPEPS event set. Validation of the new
70 method is done by comparing with the event set which is constructed using reanalysis data. The added values of
71 this new approach are also discussed and presented. The paper is organised as follows: data sets which are used
72 in this study are described in Section 2. Section 3 outlined the method that has been used to construct the TPEPS



73 event set. Results and discussions including validation and investigate the characteristic of the TPEPS event set
74 are presented in Section 4. A summary and conclusions can be found in Section 5.

75

76 **2 Data**

77 6-hourly instantaneous 10-m wind speed data in different data archives mentioned below are used in this study
78 because it is highly related to TC wind damages. The domain of this study covers the Western North Pacific
79 (WNP), east and south-east Asia spanning from 85° E to 195° E and 15° S to 75° N. The Japanese 55-year
80 Reanalysis (JRA-55) (Kobayashi et al., 2015) from 1979 until 2017 (resolution of 1.25°×1.25°) is used for
81 validation of the TPEPS event set. JRA-55 (1979-2014) is also used in parameter selection in TC identification
82 algorithm, construction of Logistic Regression Classifier (LRC) (Sect. 3.2.2), and the data in 2015-2017 is used
83 for validation of LRC. ERA-Interim (ERA-I) (Dee et al., 2011) is also used in the construction of LRC.

84 The TIGGE data archive (Bougeault et al., 2010; Swinbank et al., 2015) is used in the construction of
85 the PEPS TC event set. The TIGGE data archive has been used extensively in the study of TC activity forecast
86 (e.g. Vitart et al., 2012; Belanger et al., 2012; Halperin et al., 2013; Majumdar and Torn, 2014; Leonardo and
87 Colle, 2017; Luitel et al., 2018). TIGGE data archive consists of ~8-15-day ensemble forecast data from 10
88 numerical weather prediction centres with about 11-50 members each. In this study, only perturbed forecast
89 outputs of EPS from selected centres are used and they are Chinese Meteorological Administration (CMA),
90 European Centre for Medium-Range Weather Forecasts (ECMWF), Japanese Meteorological Agency (JMA), and
91 National Centers for Environmental Prediction (NCEP) (cf. Table 1). These four data sets are chosen because
92 they are the most complete dataset in the archive for the study period 2008-2017. Model configurations and model
93 updates are documented online at <https://confluence.ecmwf.int/display/TIGGE/Models>. ECMWF EPS is a
94 variable resolution EPS, i.e. days 1-10 were run at a higher resolution than days 11-15. For computational
95 efficiency, ECMWF EPS outputs are regridded into a lower resolution grid of 0.5625° × 0.5625°. The resolution
96 of the selected data sets ranges from 0.5625°×0.5625° to 1.25°×1.25°. Forecast lead time of each forecast outputs
97 ranges from 216 to 384 hours. Only forecast outputs, which are initialised during the main typhoon season, i.e.
98 15 May-30 November, are considered. The resultant TPEPS TC event set has data equivalent to more than 10,000
99 years of TC model data of the current climate state.

100 The International Best Track Archive for Climate Stewardship (IBTrACS) v03r10 (Knapp et al., 2010)
101 is used for validation and identification of TC events in reanalysis and TIGGE data archive. It contains all of the
102 available best track records from different centres around the globe up to year 2017. Since only part of the best
103 track records of year 2017 are archived in this version of IBTrACS, best track data from Joint Typhoon Warning
104 Centre (JTWC) is used for year 2017.

105

106 **3 Methods**

107 **3.1 Identification and characterisation of typhoon-related windstorms**



108 For identification and characterisation of typhoon-related windstorms, an impact-oriented tracking algorithm is
109 used – WiTRACK (Leckebusch et al., 2008; Kruschke, 2015). Befort et al. (2020) adapted the algorithm to
110 tropical cyclones and showed WiTRACK is well capable to identify high impact typhoon events in WNP in
111 comparable quality to more data intensive algorithms. A brief description of the general procedure to track a
112 windstorm using WiTRACK is as follows: (i) clusters with wind speed above the local threshold are identified
113 for each of the 6-hourly time step of the input dataset; (ii) clusters with size smaller than a predefined threshold
114 (*minarea*) are excluded; (iii) clusters identified in each 6-hourly time step are connected to a track using a nearest-
115 neighbour criterion with consideration of the size of the cluster; (iv) events with lifetime less than 8 6-hourly time
116 steps are removed. Majority of the settings of WiTRACK are identical to Befort et al. (2020), including the use
117 of local 98th percentile wind speed as local wind threshold, except in this study *minarea* is chosen to be 15,000
118 km². The 98th percentile wind speed is chosen because over 90% of loss events with losses above 3,000 million
119 RMB can be identified by WiTRACK as demonstrated by Befort et al. (2020). The value for *minarea* is chosen
120 based on a series of sensitivity studies for parameter selection. The output of WiTRACK contains information
121 about the characteristics of all identified windstorm events, including size of the windstorm at any given 6-hourly
122 time step, the overall footprint of extreme wind associated with the windstorm events, and storm severity index
123 (SSI; Leckebusch et al., 2008). These information are used in the identification of typhoon related pure EPS
124 windstorm events (Sect. 3.2).

125 **3.2 Identifying typhoon-related pure EPS windstorm events**

126 WiTRACK identifies windstorm events of all kind, including MEPS TCs, PEPS TCs, MEPS extratropical
127 cyclones. Therefore additional requirements are needed to identify typhoon-related PEPS TC events. 4 post-
128 processing procedures are used: (i) Geographic Filter (GF), (ii) Logistic Regression Classifier (LRC), (iii) MEPS
129 TC Identifier (MTI), and (iv) Detection at Initialisation Filter (DIF).

130 **3.2.1 Geographic Filter (GF)**

131 GF was first introduced by Befort et al. (2020). It aims to remove non-TC-related windstorms, e.g. extratropical
132 cyclones, cold surge outbreaks during the winter monsoon, and equatorial disturbances, from the event set by
133 excluding windstorm events which solely identified north of 26° N and east of 100° E, and latitudinal position
134 exclusively south of 10° N. Befort et al. (2020) found this filter can reduce the false alarm rate (i.e. the ratio
135 between number of identified non-TC related windstorms and total number of detected windstorms) of TC
136 identification in JRA-55.

137 **3.2.2 Logistic Regression Classifier (LRC)**

138 In order to reduce computational cost and increase computational efficiency, the classical methods to determine
139 whether the atmospheric disturbance is a TC or non-TC via cold/warm core determination (e.g. Hart,
140 2003; Strachan et al., 2013) are not used because these methods require multiple variable fields which increase
141 computational cost significantly. Instead, a statistical learning approach, logistic regression classifier (LRC), is
142 used to determine whether the windstorm event is related to a TC or not. Details and background information of
143 LRC can be found in Hastie et al. (2009) and the *caret* package in R is used for LRC training (Kuhn et al., 2018;
144 available online at <https://github.com/topepo/caret/>). LRC is trained using the track characteristics of the event in



145 the JRA-55 and ERA-Interim event set (1979-2014) as explanatory variables (Table 2). This combination of
146 training set is chosen based on preliminary studies of constructing an optimal classifier using different
147 combination of training set. In order to avoid issues that are associated with collinearity, a stepwise Variance
148 Inflation Factor (VIF) selection method is used to identify independent variables. 17 variables have been chosen
149 to use in the construction of LRC (Table 3). Variables that relate to changes in storm position, lifetime of a storm,
150 and mean wind field structure appear to be the most important variables in the LRC. This is expected as the
151 typical trajectory, duration, and structure of TCs and other windstorms are very different. Validation using JRA-
152 55 event set (2015-2017) have shown that the accuracy of the LRC is about 90% with low rate of false positives
153 and false negatives.

154 3.2.3 MEPS TC Identifier (MTI)

155 Since there are many replicated events of forecasted historical TCs (i.e. MEPS) in the operational forecast archive,
156 it is necessary to remove these events from our event set to avoid biases toward historical events. Instead of using
157 the criteria suggested by Osinski et al. (2016), a set of strict criteria (MTI) is used in this study. This can ensure
158 the statistics and climatology of TPEPS event set is not biased toward the historical events. The MTI eliminates
159 forecast of MPES TC events where the forecasts of those MPES TCs were initialised (i) before, and (ii) after the
160 time of MPES TC genesis (hereafter type 1 and type 2 forecast events respectively). A similarity index (SI) (Eq.
161 1) is used to eliminate type 1 forecast events:

$$162 \quad d_i = \begin{cases} d_{\text{thres}} - d & d < d_{\text{thres}} \\ 0 & d \geq d_{\text{thres}} \end{cases}, \quad (1a)$$

$$163 \quad SI = \frac{\sum_i^{t_{\text{overlap}}} d_i}{d_{\text{thres}} \times t_{\text{overlap}}}, \quad (1b)$$

164 where d is the great circle distance between position of historical TC and position of TIGGE TC at the overlap
165 time step i , d_{thres} is the maximum tolerance of d , t_{overlap} is the number of overlap time steps in which both historical
166 TC and TIGGE TC existed and it must be larger than 4. Events with SI larger than SI_{thres} are considered as MPES
167 TC events. A series of sensitivity study have been done for determining the optimal choice of parameters (not
168 shown) and the most optimal setting is $d_{\text{thres}}=900$ km and $SI_{\text{thres}} = 0.1$. Type 2 forecast events are found if the
169 separation distance between the position of historical TC and the TIGGE TC at any point of their overlap time is
170 less than 400 km. This threshold is determined by the minimum separation between historical TCs and TC in
171 JRA-55 event set.

172 3.2.4 Detection at Initialisation Filter (DIF)

173 Any events that are detected at the time of model initialisation are removed following Osinski et al. (2016). It is
174 because these events are likely to be related to pre-existing disturbances or structures that leads to their
175 development. The removal of these events ensures the TPEPS event set is independent of any pre-existing weather
176 patterns.

177 3.3 Adjustment procedure

178 More than one windstorm event could be found within a close proximity of each other over the WNP. Since the
179 clustering algorithm in WiTRACK does not have a maximum size restriction on the cluster, multiple windstorm



180 events in close proximity could be identified as one windstorm event by WiTRACK. An additional procedure is
181 used to separate these merged windstorm events. This is an iterative procedure which would check whether all
182 of the grid boxes at each 6-hr time step of the windstorm are within 1,000 km radius from the centre of the
183 windstorm cluster. If any of the event grid boxes are outside the 1,000 km radius, it will first remove these grid
184 boxes and recalculate the centre of event cluster. This procedure is repeated until there is no change in the centre
185 of cluster. This procedure addresses windstorm event with unrealistically large impact area and event SSI (ESSI).
186 The threshold radius is chosen to be 1,000 km because typical size of TC wind field is smaller than a circle of
187 1,000 km radius (Lee et al., 2010; Chan and Chan, 2011).

188 **4 Results and discussions**

189 **4.1 Statistics and Validations**

190 The detection rates of historical TCs in CMA, ECMWF, JMA, and NCEP are 91.2%, 94.7%, 89.4%, and 90.7%,
191 respectively, whereas only 54.2% of historical TCs in the period of 2008-2017 are detected in JRA-55 (Table 4).
192 Since WiTRACK is a wind threshold exceedance based detection scheme and the 98th percentile wind speed value
193 of JRA-55 within the tropical WNP is similar to these selected TIGGE data (Fig. 1), this implies JRA-55
194 underestimates the wind speed of wind field of TCs, which is in agreement with Murakami (2014). This also
195 shows these selected TIGGE outputs provide a better representation of the atmosphere. Total 515,712 TC related
196 windstorm events are detected in the selected TIGGE data set. ~38.5% of the all TPEPS events are PEPS TC
197 events (Table 5). Percentage of total TC windstorms as PEPS TCs can be treated as a proxy to quantify the
198 forecast skill of the model. Yet, this is not the focus of this study and the rest of the discussion focuses on the
199 TPEPS TC event set.

200 Figures 2 and 3 show the spatial pattern and temporal variability, respectively, of the TPEPS and JRA-
201 55 event sets. While individual model might have bias in certain spatial and temporal domain, for example the
202 region with the highest track density of JMA is at the eastern WNP in Fig. 1d in comparison to other models, and
203 NCEP failed to capture the peak activity prior 2012 in Fig. 2, the overall patterns of the TPEPS event set match
204 the JRA-55 event set. This is expected because (i) TC formation depends on the environmental conditions and
205 initial disturbance (Gray, 1977; Ritchie and Holland, 1997; Nolan, 2007). During the period of active TC season,
206 environmental conditions over WNP are usually favourable for TC formation but often there is no suitable
207 disturbance in the region. Since EPS simulates the chaotic behaviour of the atmosphere, it would forecast
208 disturbances which would be possible to form but not realised in the real atmosphere. Hence PEPS TCs can be
209 formed in those period of time over WNP; (ii) the trajectory of TCs depends mainly on the large scale
210 environmental flow of the region (Chan, 2010). This implies PEPS TCs would also follow the typical trajectory
211 of real TCs given that the large scale flow is correctly represented in the forecast models. Thus the spatial and
212 temporal patterns of the TPEPS event set match the patterns of JRA-55 event set. The spatial discrepancy near
213 the dateline between the JRA-55 event set and the TPEPS event set (Figs. 2c and 2f) can be explained by
214 considering the amount of data used in the construction of event sets. The JRA-55 event set is constructed based
215 on 39-year of reanalysis data whereas the TPEPS event set is constructed using more than 10,000 years of TC
216 model data from operational forecast models. Since both event sets are constructed from physical models (i.e.
217 GCMs), the JRA-55 event set can be considered as a subset of the TIGGE event set. Furthermore, in the region



218 0-20 °N and 160-180 °E, the 98th percentile values of JRA-55 is higher than all TIGGE models considered in this
219 study (Fig. 1). Consequently, systems with the same strength would be identified in that region in the TPEPS
220 event set but not in the JRA-55 event set.

221 Some of the examples of TPEPS TC tracks and impact footprints are shown in Fig. 4. The trajectory of
222 these TPEPS TC tracks is indistinguishable to historical TC trajectories in WNP. This shows these TPEPS TC
223 events are realistic and physically possible events. Figure 5 shows the climatological daily number distributions
224 of TCs for TPEPS TC event set and JRA-55 event set. Although the peak activities period of JMA is slightly
225 lagged behind and the over- and under-estimation of the peak of activity for CMA and NCEP are observed,
226 respectively, the seasonal cycle of TPEPS TC event set is well captured and this matches to the seasonal cycle of
227 the JRA-55 event set. This shows our new approach is capable to produce spatially and temporally realistic events.

228 In general, the temporal evolutions of the number of first storm detections of TPEPS event set during the
229 integration time has an increasing trend in the short lead time followed by a roughly constant behaviour (Fig. 6).
230 In short lead time (i.e. close to initialisation of forecast), the true state of the atmosphere is well simulated by
231 forecast models, thus EPSs are likely to produce storms that actually occurred (i.e. MEPS storms) and less likely
232 to produce PEPS storms (Osinski et al., 2016). As lead time increases, more PEPS storms are produced due to
233 increasing uncertainty of the state and the chaotic behaviour of the atmosphere in EPSs. When EPS has no
234 memory of the initialisation state of the atmosphere, the probability distribution of formation of PEPS TCs
235 becomes a uniform distribution.

236 The overall impact of any storm is related to the many factors for example lifetime of the storm, the size
237 of the storm, and the intensity (or strength) of the storm (e.g. Vickery et al., 2000; Mori and Takemi, 2016; Kim
238 and Lee, 2019). Here we investigate whether there are systematic biases in the TPEPS TC event set which would
239 affect these quantities. The lifetime distribution of TPEPS TCs matches to the JRA-55 event set but proportionally
240 overestimates for short-lived TCs and underestimates for long-lived TCs (Fig. 7a). These differences are the
241 consequence of the finite simulation time in forecast models. If the same restriction (i.e. finite simulation time
242 window) is applied to the JRA-55 TC event set (grey shaded areas in Fig. 7), the lifetime distribution of TPEPS
243 TCs would be in good agreement to the JRA-55 TCs. Similar conclusion can be reached in the comparison of the
244 distribution of time required to reach lifetime maximum intensity (LMI) (Fig. 7b). However, finite simulation
245 time of EPSs cannot explain the difference in the distribution of impact area between TPEPS and JRA-55 event
246 sets despite they have the same type of distribution (Fig. 7c). The difference in the distributions of impact area
247 maybe due to the fact that wind speed of the TC wind fields is underestimated in JRA-55 as discussed above.
248 Consequently, many weaker TCs, which would have small impact areas, are not detected and thus they are not
249 necessarily included in the JRA-55 TC event set.

250 **4.2 Robust TC risk assessment**

251 To demonstrate the benefit of our approach, TC records in IBTrACS, JRA-55 TC event set, and TPEPS TC event
252 set are stratified into intensity classes according to their lifetime maximum intensity (c.f. Table 6). Since
253 WiTRACK is an impact-oriented, wind speed percentile based tracking scheme which tracks TCs with potential
254 impact (Befort et al., 2020). Many of the low impact TCs (i.e. TCs in the Tropical Depression and Tropical Storm
255 (TD&TS) category) are not detected and thus not included in the TPEPS TC event set. Focusing onto the



256 categories of high impact TC, i.e. Typhoon (TY), Very Strong Typhoon (VST), and Violent Typhoon (VTY), the
257 TPEPS event set contains 302.14, 102.54, and 77.02 times more TY, VST, and VTY than the IBTrACS records,
258 respectively. This means our new approach can capture much more extremely high impact events such that a
259 more robust analysis of extreme TC events can be done.

260 The key advantage of this new approach is that it constructs a physically consistent and high information
261 content TC event set with good and realistic representation of the current climate state using a computationally
262 inexpensive algorithm. Since more physically consistent and physically possible TCs are included, more extreme
263 events can be captured in the TPEPS event set. Consequently, a robust TC risk assessment can be obtained. Some
264 of the examples are presented in this subsection.

265 Figure 8 shows the location of first detection of TCs with LMI at least typhoon strength, which made
266 landfall within the given domain (105-180° E, 0-30° N) for TPEPS and JRA-55 TC event set. The spatial pattern
267 of the TPEPS TC event set (Fig. 8f) matches the spatial pattern of the JRA-55 TC event set. The data in the JRA-
268 55 TC event set are sparse and it does not provide sufficient information about whether TCs, which made landfall
269 in this region, are typically first identified in the WNP or in the South China Sea (SCS). TPEPS event set, on the
270 other hand, provides a clearer picture and suggests events, which made landfall in this domain, are typically first
271 identified in the SCS and western WNP. This is consistent with the known climatology. As TCs within the SCS
272 and western WNP usually follow the western and northwestern trajectory and subsequently made landfall over
273 the Vietnam, south and southeast mainland China, Taiwan, and the Philippines.

274 Figure 9 shows the number of TC landfall events, which made landfall with at least typhoon strength,
275 with the focus of southern and southeast mainland China, and Taiwan. Much more landfall events have been
276 captured by TPEPS TC event set (11449) than the JRA-55 TC event set (100). The spatial distribution of TPEPS
277 TCs is in good agreement with the JRA-55 TCs. TCs, which made landfall with at least typhoon strength, are
278 more likely to made landfall along the coast of the southern Fujian Province and the eastern Guangdong Province
279 than any other coastal area of South and Southeast mainland China. Furthermore, higher TC landfall frequency
280 is observed on the side of islands (i.e. Hainan Island and Taiwan) which faces the open ocean than the other side
281 of islands. This is consistent with observations. The TPEPS TC event set also provides information about the
282 frequency of TC landfall at locations where no landfall events had observed in the JRA-55 event set, e.g. locations
283 along the coastline of Guangdong Province.

284 **4.3 Application**

285 The TPEPS event set is constructed based on physical models, i.e. GCMs, which provide a good representation
286 of the atmosphere of the real world. The wind field associates to a TPEPS event is realistic and local effects, such
287 as local topography, have been taken into account. This implies the wind information of the TPEPS event set can
288 be used for estimates return periods of local extreme wind events associated with typhoon with high confidence.
289 Figure 10 shows the number of TC-related 6-hourly extreme wind (i.e. wind speed higher than the local 98th
290 percentile climatological wind speed) data entries in each of the grid box within Guangdong Province in the
291 Southern China. The JRA-55 event set can only construct a TC-related 6-hourly extreme distribution with ~25
292 (inland) and ~325 (coastal) data entries whereas such distribution can be constructed with at least 500 to over
293 28,000 data entries using the TPEPS TC event set. This implies the estimated return period using the TPEPS TC



294 event set would be more reliable than using the JRA-55 event set and similarly the observation data alone. This
295 is demonstrated as follows.

296 Four surface observation stations are chosen for this demonstration, they are Baiyun International Airport
297 (BAIYUN INTL; 23.392° N, 113.299° E; from 1945-2019), Baoan International Airport (BAOAN INTL; 22.639°
298 N, 113.811° E; from 1957-2019), Shanwei (22.783° N, 115.367° E; from 1956-2019), and Shangchuan Dao
299 (21.733° N, 112.767° E; from 1959-2019). For each selected surface station, the grid box of each EPS that
300 corresponds to the surface station is identified (Fig.11). Resolution of models is known to be a factor to limit the
301 wind speed of TCs (Bengtsson et al., 2007). This means for the same TC, the associated wind speed would be
302 lower in low resolution model and higher for high resolution model. In order to utilise the extreme wind
303 information from EPSs with different resolution, the cube of 98th percentile relative exceedance of wind speed
304 (EXCE) is used. Since EXCE is a ratio, it is a resolution independent quantity and the tail behaviours of the
305 EXCE distribution for these models are similar, which is in agreement with Osinski et al. (2016). Information
306 from different models can be combined using EXCE. EXCE entries, which correspond to TC in the TPEPS TC
307 event set, are extracted for those grid boxes. This forms a set of “observations” of the impacts of high impact TCs
308 at those grid boxes in the model space. We assume all of the EXCE entries are independent and identically
309 distributed (iid) random variables. This is a reasonable assumption, due to the fast moving nature of TCs, diverse
310 possible direction of the movement of wind field, and rapid decay of wind field over land for a 6-hour interval,
311 local observations often have only one extreme wind observations of a TC event. In order to translate this
312 information to the physical world, quantile mapping is used for mapping EXCE to the observed surface wind
313 speed which exceeded local climatological 98th percentile. Historical in situ surface wind data are obtained from
314 the Integrated Surface Database (ISD) (Smith et al., 2011). Quantile mapping is done using the R package *qmap*
315 (Gudmundsson et al., 2012; Gudmundsson, 2016). Due to different geographic configuration and climatology of
316 each in situ observation station, different quantile mapping strategies have been employed. The optimal strategy
317 is chosen based on minimisation of the root-mean-square-error (RMSE) of (see Gudmundsson (2016) for more
318 details). Using above information, the return period-return level plot (using threshold exceedance approach) is
319 constructed using the R package *extRemes* (Gilleland and Katz, 2016). For detail discussion of calculation of
320 return period and return level, readers are referred to Elsner et al. (2006), Jagger and Elsner (2006), and Gilleland
321 and Katz (2016). Figure 12 shows the return period-return level plot of 4 selected stations which are derived using
322 our proposed approach with the TPEPS event set and using in situ observational data. The width of the 95%
323 confidence interval which is calculated using our proposed approach is much sharper than the 95% confidence
324 interval which is calculated using in situ observational data. In other words, the uncertainty can be reduced by
325 using the TPEPS event set because more observations are used in the calculation.

326 The above application of the TPEPS event set can provide crucial information for the DRR community.
327 As discussed in the introduction, typhoon parametric insurance can be an effective financial instrument for
328 typhoon risk transfer. However, an effective typhoon parametric insurance requires a robust trigger point, which
329 is determined by the meteorological information, e.g. wind speed. If the trigger point is too high, disbursements
330 would not be made even if a catastrophic meteorological disaster has occurred, i.e. under-compensation; If the
331 trigger point is too low, disbursements would be made even if no catastrophic event has occurred. Using the



332 TPEPS event set, the estimated return period has smaller uncertainty than the estimation made by in situ
333 observational data, such that an optimal trigger point for typhoon parametric insurance can be determined.

334 **5 Summary and Conclusions**

335 In this study, a new and efficient method to produce a physically consistent TC event set with high information
336 content in the WNP has been presented. This is achieved by applying an objective impact-oriented windstorm
337 identification algorithm – WiTRACK, on 6-hourly 10-m horizontal wind field of selected ensemble data set from
338 a multi-centre grand ensemble data archive – TIGGE. Several sensitivity tests with different parameter settings
339 are done using JRA-55 data to obtain the optimal setup for WiTRACK. Since WiTRACK can identify all types
340 of windstorm events, 4 post-processing procedures are used to identify PEPS TCs, these procedures include a
341 geographic filter and logistics regression classifier. The TPEPS event set has the climatological spatial and
342 temporal pattern of TCs which match to the historical climatological pattern of TC in WNP. More than 302, 102,
343 and 77 times of TY, VSTY, and VTY, respectively, are found in the TPEPS TC event set in comparison to the
344 IBTrACS record. A robust representation of extreme TC events in WNP can be obtained using the TPEPS TC
345 event set because of the high number of physically consistent extreme events. Consequently, a robust hazard risk
346 assessment of land-affecting typhoons in the WNP can be produced using the event set constructed by this new
347 method. Furthermore, the return-period of typhoon-related extreme wind events e.g. Typhoon Haiyan (2013) and
348 Typhoon Mangkhut (2018), can be determined with sharper confidence intervals in a similar manner as Walz and
349 Leckebusch (2019). As a result, policymakers and related stakeholders can improve the current typhoon related
350 disaster reduction and mitigation strategy. Furthermore a robust trigger point for parametric typhoon hazard
351 insurance can be determined using our proposed approach by reducing the uncertainty of estimated return period
352 of a meteorological extreme event.

353 The TC event set constructed using the method described in this paper has several unique properties in comparison
354 to the TC event set constructed by other methods (Vickery et al., 2000; Emanuel et al., 2006; Rumpf et al.,
355 2009; Kim and Lee, 2019):

356 (i) Many methods in the literature (Emanuel et al., 2006; Rumpf et al., 2009) use historical best track data to
357 construct a spatial probability function that determine the genesis location of synthetic TCs and a parametric track
358 model, that matches to the historical observations, to determine the movement of synthetic TCs. Consequently,
359 these synthetic tracks are highly likely to be identified in the region where TCs were identified from the historical
360 observations and highly unlikely in the region where TCs were never identified but physically possible. In contrast,
361 TPEPS TCs are detected at any physically possible locations over the WNP. The TPEPS event set includes events
362 which are unlikely but physically possible. This provides an important and unique advantage for typhoon risk
363 assessment.

364 (ii) In the literature, the structure of wind field of synthetic TCs follows a predefined, analytical model, e.g.
365 parametric vortex structure developed by Holland (1980) or modified Rankine vortex. For the TPEPS event set,
366 complex physical processes in GCMs determine the structure of wind field of TCs, therefore the structure of wind
367 field of TCs is realistic. This is an advantage for robust wind risk assessment of land-affecting TCs because the
368 resultant wind field includes the complex atmosphere-land interaction which depends on the local topography.



369 Consequently, the TPEPS event set can be used as additional observations for the estimation of return period of TC-
370 related extreme wind as demonstrated above.

371 (iii) Many of the TC risk assessments are done based on wind risk, and/or wind-induced coastal risk but not TC-
372 related precipitation risk (Vickery et al., 2000; Emanuel et al., 2006; Rumpf et al., 2009; Mendelsohn et al.,
373 2012; Mori and Takemi, 2016; Marsooli et al., 2019; Kim and Lee, 2019). A reason is that historical damages
374 due to TC-related wind are much better documented than TC-related precipitation damages (Emanuel et al., 2006).
375 However, damages due to TC-related precipitation, e.g. flooding, should not be ignored. Based on the payout of
376 National Flood Insurance Program of the United States for the flood event of Hurricane Ike (2008), Smith and
377 Katz (2013) estimated the insured flood damage as 5.376 billion USD. Furthermore, some of the high impact
378 TCs in WNP have typical typhoon intensity but the amount of rainfall is extremely high, e.g. Typhoon Morakot
379 (2009) (Wu, 2012). Since precipitation is one of the output variables of these medium range ensemble forecasts,
380 precipitation-related impact can be examined by integrating the realistic precipitation information from forecast
381 outputs into the TPEPS event set. Furthermore a spatial distribution of TC related hazard, e.g. extreme wind and
382 extreme precipitation, of the TPEPS event set can be constructed using the notion of TC hazard footprint (Chen
383 et al., 2018). Consequently, a more thorough typhoon risk assessment can be achieved. This is currently under
384 our investigation.

385

386 *Data availability.* JRA-55 (Kobayashi et al., 2015) and ERA-I (Dee et al., 2011) are freely available for academic
387 use at the UCAR Research Data Archive: <https://rda.ucar.edu/datasets>. The TIGGE dataset (Bougeault et al.,
388 2010; Swinbank et al., 2015) used in this study can be accessed through ECMWF server:
389 <https://apps.ecmwf.int/datasets/data/tigge/levtype=sfc/type=pf/>. IBTrACS (Knapp et al., 2010) and ISD (Smith
390 et al., 2011) are available at the United States National Centers for Environmental Information, National oceanic
391 and Atmospheric Administration: <https://www.ncdc.noaa.gov/ibtracs/index.php>, and
392 <https://www.ncdc.noaa.gov/isd>, respectively. JTWC best track data used in this study is obtained from the United
393 States Navy Website: <https://www.metoc.navy.mil/jtwc/jtwc.html?best-tracks>.

394

395 *Author contribution.* KSN and GCL originated the idea, developed the methodology, performed data analysis, and
396 wrote the paper.

397

398 *Competing interests.* The authors declare that they have no conflict of interest.

399

400 *Acknowledgments.* The authors thank Drs. D. Befort and M. Angus for valuable discussion. This work was
401 supported by the Building Resilience to Natural Disasters using Financial Instruments grant INPAIS (Integrated
402 Threshold Development for Parametric Insurance Solutions for Guangdong Province China, Grant Ref:
403 NE/R014264/1, through Natural Environment Research Council (NERC). The computations described in this
404 paper were performed using the BlueBEAR HPC service at the University of Birmingham.



405 **References**

- 406 Befort, D. J., Kruschke, T., and Leckebusch, G. C.: Objective Identification of Potentially Damaging Tropical
407 Cyclones over the Western North Pacific, Environmental Research Communications, ERC-100169,
408 accepted 28 February 2020, 2020.
- 409 Belanger, J. I., Webster, P. J., Curry, J. A., and Jelinek, M. T.: Extended Prediction of North Indian Ocean
410 Tropical Cyclones, *Weather and Forecasting*, 27, 757-769, 10.1175/WAF-D-11-00083.1, 2012.
- 411 Bengtsson, L., Hodges, K. I., and Esch, M.: Tropical cyclones in a T159 resolution global climate model:
412 Comparison with observations and re-analyses, *Tellus A*, 59, 396-416, 2007.
- 413 Bougeault, P., Toth, Z., Bishop, C., Brown, B., Burridge, D., Chen, D. H., Ebert, B., Fuentes, M., Hamill, T. M.,
414 Mylne, K., Nicolau, J., Paccagnella, T., Park, Y.-Y., Parsons, D., Raoult, B., Schuster, D., Dias, P. S.,
415 Swinbank, R., Takeuchi, Y., Tennant, W., Wilson, L., and Worley, S.: The THORPEX Interactive
416 Grand Global Ensemble, *B Am Meteorol Soc*, 91, 1059-1072, 10.1175/2010BAMS2853.1, 2010.
- 417 Chan, J. C. L.: Movement of Tropical Cyclones, in: *Global Perspectives on Tropical Cyclones*, World Scientific
418 Series on Asia-Pacific Weather and Climate, Volume 4, World Scientific, 133-148, 2010.
- 419 Chan, K. T. F., and Chan, J. C. L.: Size and Strength of Tropical Cyclones as Inferred from QuikSCAT Data,
420 *Mon Weather Rev*, 140, 811-824, 10.1175/MWR-D-10-05062.1, 2011.
- 421 Chen, W., Lu, Y., Sun, S., Duan, Y., and Leckebusch, G. C.: Hazard Footprint-Based Normalization of
422 Economic Losses from Tropical Cyclones in China During 1983–2015, *International Journal of*
423 *Disaster Risk Science*, 9, 195-206, 10.1007/s13753-018-0172-y, 2018.
- 424 Dee, D. P., Uppala, S. M., Simmons, A. J., Berrisford, P., Poli, P., Kobayashi, S., Andrae, U., Balmaseda, M.
425 A., Balsamo, G., Bauer, P., Bechtold, P., Beljaars, A. C. M., van de Berg, L., Bidlot, J., Bormann, N.,
426 Delsol, C., Dragani, R., Fuentes, M., Geer, A. J., Haimberger, L., Healy, S. B., Hersbach, H., Hólm, E.
427 V., Isaksen, I., Kållberg, P., Köhler, M., Matricardi, M., McNally, A. P., Monge-Sanz, B. M.,
428 Morcrette, J. J., Park, B. K., Peubey, C., de Rosnay, P., Tavolato, C., Thépaut, J. N., and Vitart, F.: The
429 ERA-Interim reanalysis: configuration and performance of the data assimilation system, *Q J Roy*
430 *Meteor Soc*, 137, 553-597, 10.1002/qj.828, 2011.
- 431 Desai, B., Maskrey, A., Peduzzi, P., De Bono, A., and Herold, C.: Making Development Sustainable: The
432 Future of Disaster Risk Management, *Global Assessment Report on Disaster Risk Reduction*, United
433 Nations Office for Disaster Risk Reduction (UNISDR), Genève, Suisse, Geneva: UNISDR, 2015.
- 434 Elsner, J. B., Jagger, T. H., and Tsonis, A. A.: Estimated return periods for Hurricane Katrina, *Geophys Res*
435 *Lett*, 33, 10.1029/2005GL025452, 2006.
- 436 Emanuel, K.: Climate and tropical cyclone activity: A new model downscaling approach, *J Climate*, 19, 4797-
437 4802, Doi 10.1175/Jcli3908.1, 2006.
- 438 Emanuel, K., Ravela, S., Vivant, E., and Risi, C.: A statistical deterministic approach to hurricane risk
439 assessment, *B Am Meteorol Soc*, 87, 299-314, 10.1175/Bams-87-3-299, 2006.
- 440 Gilleland, E., and Katz, R. W.: extRemes 2.0: An Extreme Value Analysis Package in R, *Journal of Statistical*
441 *Software*; Vol 1, Issue 8 (2016), 10.18637/jss.v072.i08, 2016.
- 442 Glauber, J. W.: Crop Insurance Reconsidered, *American Journal of Agricultural Economics*, 86, 1179-1195,
443 10.1111/j.0002-9092.2004.00663.x, 2004.
- 444 Gray, W. M.: Tropical Cyclone Genesis in the Western North Pacific, *J Meteorol Soc Jpn*, 55, 465-482, 1977.



- 445 Gudmundsson, L., Bremnes, J. B., Haugen, J. E., and Engen-Skaugen, T.: Technical Note: Downscaling RCM
446 precipitation to the station scale using statistical transformations – a comparison of methods,
447 *Hydrol. Earth Syst. Sci.*, 16, 3383-3390, 10.5194/hess-16-3383-2012, 2012.
- 448 Gudmundsson, L.: qmap: Statistical transformations for post-processing climate model output. R package
449 version 1.0-4. 2016.
- 450 Halperin, D. J., Fuelberg, H. E., Hart, R. E., Cossuth, J. H., Sura, P., and Pasch, R. J.: An Evaluation of Tropical
451 Cyclone Genesis Forecasts from Global Numerical Models, *Weather and Forecasting*, 28, 1423-1445,
452 10.1175/WAF-D-13-00008.1, 2013.
- 453 Hart, R. E.: A cyclone phase space derived from thermal wind and thermal asymmetry, *Mon Weather Rev*, 131,
454 585-616, Doi 10.1175/1520-0493(2003)131<0585:Acpsdf>2.0.Co;2, 2003.
- 455 Hastie, T., Tibshirani, R., and Friedman, J.: *The Elements of Statistical Learning*, Springer Series in Statistics,
456 Springer-Verlag New York, 745 pp., 2009.
- 457 Holland, G. J.: An Analytic Model of the Wind and Pressure Profiles in Hurricanes, *Mon Weather Rev*, 108,
458 1212-1218, 10.1175/1520-0493(1980)108<1212:AAMOTW>2.0.CO;2, 1980.
- 459 IPCC: *Managing the risks of extreme events and disasters to advance climate change adaptation*, Cambridge, A
460 special report of Working Groups I and II of the Intergovernmental Panel on Climate Change, 2012.
- 461 Jagger, T. H., and Elsner, J. B.: Climatology Models for Extreme Hurricane Winds near the United States, *J*
462 *Climate*, 19, 3220-3236, 10.1175/JCLI3913.1, 2006.
- 463 Kim, G. Y., and Lee, S.: Prediction of extreme wind by stochastic typhoon model considering climate change,
464 *Journal of Wind Engineering and Industrial Aerodynamics*, 192, 17-30, 10.1016/j.jweia.2019.05.003,
465 2019.
- 466 Knapp, K. R., Kruk, M. C., Levinson, D. H., Diamond, H. J., and Neumann, C. J.: The International Best Track
467 Archive for Climate Stewardship (IBTrACS) Unifying Tropical Cyclone Data, *B Am Meteorol Soc*,
468 91, 363-376, Doi 10.1175/2009bams2755.1, 2010.
- 469 Kobayashi, S., Ota, Y., Harada, Y., Ebata, A., Moriya, M., Onoda, H., Onogi, K., Kamahori, H., Kobayashi, C.,
470 Endo, H., Miyaoka, K., and Takahashi, K.: The JRA-55 Reanalysis: General Specifications and Basic
471 Characteristics, *Journal of the Meteorological Society of Japan. Ser. II*, 93, 5-48, 10.2151/jmsj.2015-
472 001, 2015.
- 473 Kruschke, T.: *Winter wind storms: Identification, verification of decadal predictions, and regionalization*,
474 *Doktors der Naturwissenschaften, Institut für Meteorologie, Freie Universität Berlin*, 181 pp., 2015.
- 475 Kuhn, M., Wing, J., Weston, S., Williams, A., Keefer, C., Engelhardt, A., Cooper, T., Mayer, Z., Kenkel, B.,
476 Benesty, M., Lescarbeau, R., Ziem, A., Scrucca, L., Tang, Y., Candan, C., and Hunt, T.: *Classification*
477 *and Regression Training*. 2018.
- 478 Leckebusch, G. C., Renggli, D., and Ulbrich, U.: Development and Application of an Objective Storm Severity
479 Measure for the Northeast Atlantic Region, *Meteorologische Zeitschrift*, 17, 575-587, 10.1127/0941-
480 2948/2008/0323, 2008.
- 481 Lee, C.-S., Cheung, K. K. W., Fang, W.-T., and Elsberry, R. L.: Initial Maintenance of Tropical Cyclone Size in
482 the Western North Pacific, *Mon Weather Rev*, 138, 3207-3223, 10.1175/2010MWR3023.1, 2010.



- 483 Lemecke, G.: A resilient world: NatCat parametric insurance solutions for China's Provincial Government, Sigma
484 event 2017: Catastrophes-Protecting the uninsured. Solutions for a resilient world, Zurich, Switzerland,
485 6-7 April, 2017.
- 486 Leonardo, N. M., and Colle, B. A.: Verification of Multimodel Ensemble Forecasts of North Atlantic Tropical
487 Cyclones, *Weather and Forecasting*, 32, 2083-2101, 10.1175/WAF-D-17-0058.1, 2017.
- 488 Luitel, B., Villarini, G., and Vecchi, G. A.: Verification of the skill of numerical weather prediction models in
489 forecasting rainfall from U.S. landfalling tropical cyclones, *Journal of Hydrology*, 556, 1026-1037,
490 10.1016/j.jhydrol.2016.09.019, 2018.
- 491 Majumdar, S. J., and Torn, R. D.: Probabilistic Verification of Global and Mesoscale Ensemble Forecasts of
492 Tropical Cyclogenesis, *Weather and Forecasting*, 29, 1181-1198, 10.1175/WAF-D-14-00028.1, 2014.
- 493 Marsooli, R., Lin, N., Emanuel, K., and Feng, K.: Climate change exacerbates hurricane flood hazards along US
494 Atlantic and Gulf Coasts in spatially varying patterns, *Nature Communications*, 10, 3785,
495 10.1038/s41467-019-11755-z, 2019.
- 496 Mendelsohn, R., Emanuel, K., Chonabayashi, S., and Bakkensen, L.: The impact of climate change on global
497 tropical cyclone damage, *Nature Climate Change*, 2, 205-209, 10.1038/nclimate1357, 2012.
- 498 Mori, N., and Takemi, T.: Impact assessment of coastal hazards due to future changes of tropical cyclones in the
499 North Pacific Ocean, *Weather and Climate Extremes*, 11, 53-69, 10.1016/j.wace.2015.09.002, 2016.
- 500 Murakami, H.: Tropical cyclones in reanalysis data sets, *Geophys Res Lett*, 41, 2133-2141,
501 10.1002/2014GL059519, 2014.
- 502 Nolan, D. S.: What is the trigger for tropical cyclogenesis?, *Aust. Met. Mag.*, 56, 241-266, 2007.
- 503 Osinski, R., Lorenz, P., Kruschke, T., Voigt, M., Ulbrich, U., Leckebusch, G. C., Faust, E., Hofherr, T., and
504 Majewski, D.: An approach to build an event set of European windstorms based on ECMWF EPS, *Nat.*
505 *Hazards Earth Syst. Sci.*, 16, 255-268, 10.5194/nhess-16-255-2016, 2016.
- 506 Ritchie, E. A., and Holland, G. J.: Scale interactions during the formation of Typhoon Irving, *Mon Weather*
507 *Rev.*, 125, 1377-1396, 1997.
- 508 Rumpf, J., Weindl, H., Hölpe, P., Rauch, E., and Schmidt, V.: Stochastic modelling of tropical cyclone tracks,
509 *Mathematical Methods of Operations Research*, 66, 475-490, 10.1007/s00186-007-0168-7, 2007.
- 510 Rumpf, J., Weindl, H., Hölpe, P., Rauch, E., and Schmidt, V.: Tropical cyclone hazard assessment using model-
511 based track simulation, *Nat Hazards*, 48, 383-398, 10.1007/s11069-008-9268-9, 2009.
- 512 Shi, P.: On the role of government in integrated disaster risk governance—Based on practices in China,
513 *International Journal of Disaster Risk Science*, 3, 139-146, 10.1007/s13753-012-0014-2, 2012.
- 514 Smith, A., Lott, N., and Vose, R.: The Integrated Surface Database: Recent Developments and Partnerships, *B*
515 *Am Meteorol Soc*, 92, 704-708, 10.1175/2011BAMS3015.1, 2011.
- 516 Smith, A. B., and Katz, R. W.: US billion-dollar weather and climate disasters: data sources, trends, accuracy
517 and biases, *Nat Hazards*, 67, 387-410, 10.1007/s11069-013-0566-5, 2013.
- 518 Strachan, J., Vidale, P. L., Hodges, K., Roberts, M., and Demory, M.-E.: Investigating Global Tropical Cyclone
519 Activity with a Hierarchy of AGCMs: The Role of Model Resolution, *J Climate*, 26, 133-152,
520 10.1175/JCLI-D-12-00012.1, 2013.



- 521 Sun, B., Guo, C., and Cornelis van Kooten, G.: Hedging weather risk for corn production in Northeastern China:
522 The efficiency of weather-indexed insurance, *Agricultural Finance Review*, 74, 555-572,
523 10.1108/AFR-01-2014-0001, 2014.
- 524 Swinbank, R., Kyouda, M., Buchanan, P., Froude, L., Hamill, T. M., Hewson, T. D., Keller, J. H., Matsueda,
525 M., Methven, J., Pappenberger, F., Scheuerer, M., Tittley, H. A., Wilson, L., and Yamaguchi, M.: The
526 TIGGE Project and Its Achievements, *B Am Meteorol Soc*, 97, 49-67, 10.1175/BAMS-D-13-00191.1,
527 2015.
- 528 Vickery, P. J., Skerlj, P. F., and Twisdale, L. A.: Simulation of Hurricane Risk in the U.S. Using Empirical
529 Track Model, *Journal of Structural Engineering*, 126, 1222-1237, 10.1061/(ASCE)0733-
530 9445(2000)126:10(1222), 2000.
- 531 Vitart, F., Prates, F., Bonet, A., and Sahin, C.: New tropical cyclone products on the web, *ECMWF Newsletter*,
532 130, 2012.
- 533 Walz, M. A., and Leckebusch, G. C.: Loss potentials based on an ensemble forecast: How likely are winter
534 windstorm losses similar to 1990?, *Atmos Sci Lett*, 20, e891, 10.1002/asl.891, 2019.
- 535 WMO: Member report [China], ESCAP/WMO Typhoon Committee 13th Integrated Workshop, 2018.
- 536 WMO: Typhoon Committee Operational Manual, World Meteorological Organization, World Meteorological
537 Organization, 2019.
- 538 Wu, C.-C.: Typhoon Morakot: Key Findings from the Journal TAO for Improving Prediction of Extreme Rains
539 at Landfall, *B Am Meteorol Soc*, 94, 155-160, 10.1175/BAMS-D-11-00155.1, 2012.
- 540 Ye, T., Wang, Y., Wu, B., Shi, P., Wang, M., and Hu, X.: Government Investment in Disaster Risk Reduction
541 Based on a Probabilistic Risk Model: A Case Study of Typhoon Disasters in Shenzhen, China,
542 *International Journal of Disaster Risk Science*, 7, 123-137, 10.1007/s13753-016-0092-7, 2016.
- 543 Ye, T., Li, Y., Gao, Y., Wang, J., and Yi, M.: Designing index-based livestock insurance for managing snow
544 disaster risk in Eastern Inner Mongolia, China, *International Journal of Disaster Risk Reduction*, 23,
545 160-168, 10.1016/j.ijdr.2017.04.013, 2017.
- 546
- 547



548 **Tables**

Centre	Number of members	Runs per day	Resolution	Implementation date	Forecast lead time (hr)
CMA	14	2 (00, 12 UTC)	0.5625°×0.5625°	20070515	240
		2 (00, 12 UTC)		20140805	360
ECMWF	50	2 (00, 12 UTC)	0.5625°×0.5625°	20061001	360
JMA	50	1 (12 UTC)	1.25° × 1.25°	20060301	216
	50	1 (12 UTC)		20130328	264
	26	2 (0, 12 UTC)		20140226	264
NCEP	20	4 (0, 6, 12, 18 UTC)	1.0° × 1.0°	20070327	384

549

550 **Table 1.** Information of selected data sources from TIGGE archive.

551



Variables
Time average of area of cluster
Time average of longitude of cluster centre
Time average of latitude of cluster centre
Time average of maximum extent of cluster
Time average of mean wind speed
Time average of standard deviation of wind speed
Time average of minimum wind speed
Time average of maximum wind speed
Time average of longitude of location of maximum wind
Time average of latitude of location of maximum wind
Time average of storm severity index (SSI)
Standard deviation of time series of area of cluster
Standard deviation of time series of longitude of cluster centre
Standard deviation of time series of latitude of cluster centre
Standard deviation of time series of maximum extent of cluster
Standard deviation of time series of mean wind speed
Standard deviation of time series of standard deviation of wind speed
Standard deviation of time series of minimum wind speed
Standard deviation of time series of maximum wind speed
Standard deviation of time series of longitude of location of maximum wind
Standard deviation of time series of latitude of location of maximum wind
Standard deviation of time series of storm severity index
Number of 6-hourly time steps
Area of windstorm event footprint
Event SSI
Difference of latitude between the initial and final locations
Difference of longitude between the initial and final locations
Total distance travelled

552

553 **Table 2.** List of explanatory variables which can be obtained from the WiTRACK output.

554



Variable	t-value
Difference of latitude between the initial and final locations	12.5707
Difference of longitude between the initial and final locations	9.9983
Time average of standard deviation of wind speed	9.3709
Time average of minimum wind speed	8.5015
Time average of maximum extent of cluster	5.1416
Number of 6-hourly time steps	4.8719
Standard deviation of times series of latitude of location of maximum wind	3.4302
Standard deviation of times series of mean wind speed	2.3640
Standard deviation of times series of area of cluster	2.2447
Event SSI	1.9621
Standard deviation of times series of maximum extent of cluster	1.7922
Time average of latitude of cluster centre	1.4493
Standard deviation of time series of SSI	0.9980
Standard deviation of times series of longitude of location of maximum wind	0.9237
Standard deviation of times series of standard deviation of wind speed	0.7268
Time average of longitude of location of maximum wind	0.4204
Standard deviation of time series of minimum wind speed	0.2613

555

556 **Table 3.** List of explanatory variables and their associated t-value which are used in the construction of LRC.

557



Year	IBTrACS	CMA	ECMWF	JMA	NCEP	JRA-55
2008	21	19	19	19	17	10
2009	22	20	20	20	14	10
2010	13	13	13	13	13	6
2011	21	19	20	17	19	14
2012	24	23	23	23	23	16
2013	29	28	28	27	28	15
2014	19	12	17	17	17	13
2015	22	20	21	20	21	17
2016	26	25	25	24	25	13
2017	30	28	29	23	29	9
Total	227	207	215	203	206	123
Detection Rate		91.2%	94.7%	89.4%	90.7%	54.2%

558

559 **Table 4.** Number of historical TCs identified.

560



Centres	Number of TC windstorms	Number of Pure EPS TCs	% of TC windstorms as pure EPS TCs
CMA	39535	13322	33.7
ECMWF	215737	74091	34.3
JMA	56537	14964	26.5
NCEP	203903	96052	47.1

561

562 **Table 5.** Statistics of TCs in the selected TIGGE data.

563



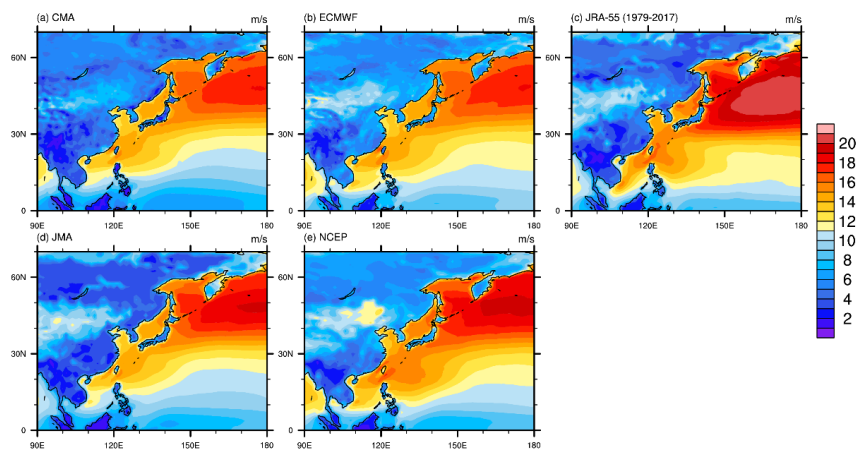
Intensity Class	IBTrACS	JRA-55	TPEPS
TD&TS	252	32	27643
STS	208	126	70759
TY	231	254	69794
VSTY	231	193	23686
VTY	85	63	6547
Total	1007	668	198429

564

565 **Table 6.** Number of TC records in IBTrACS, JRA-55 TC event set, and TPEPS TC event set, for different
566 intensity classes. The classes are Tropical Depression (TD) and Tropical Storm (TS), Severe Tropical Storm
567 (STS), Typhoon (TY), Very Strong Typhoon (VST), and Violent Typhoon (VTY). The intensity classes for
568 IBTrACS are defined according to WMO (2019). The intensity classes for JRA-55 TC and TPEPS TC are derived
569 from the WMO (2019) intensity classes by using quantile mapping of intensity records of JRA-55 TC and
570 IBTrACS records.



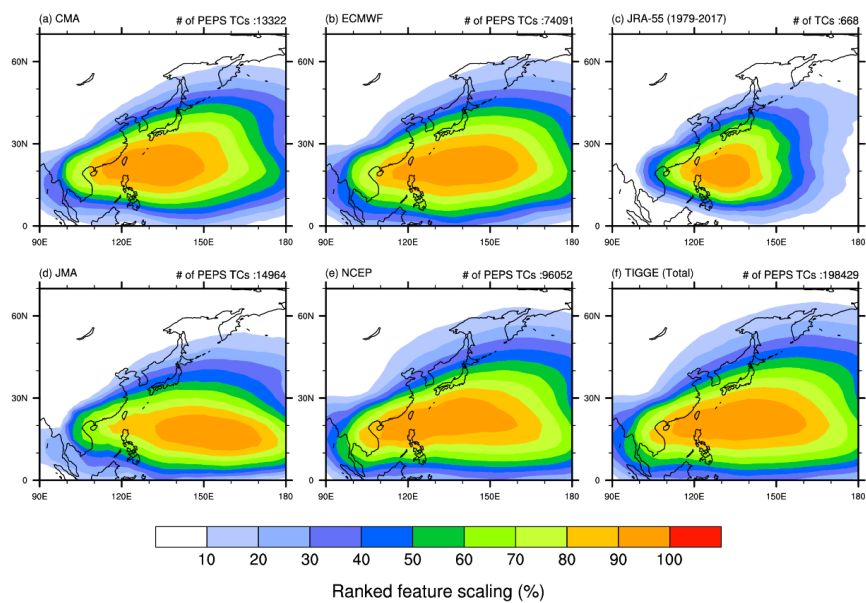
571 **Figures**



572

573 **Figure 1.** Local 98th percentile wind speed for each grid box in the region for TIGGE: (a) CMA, (b) ECMWF, (d)
574 JMA, (e) NCEP, and (c) JRA-55.

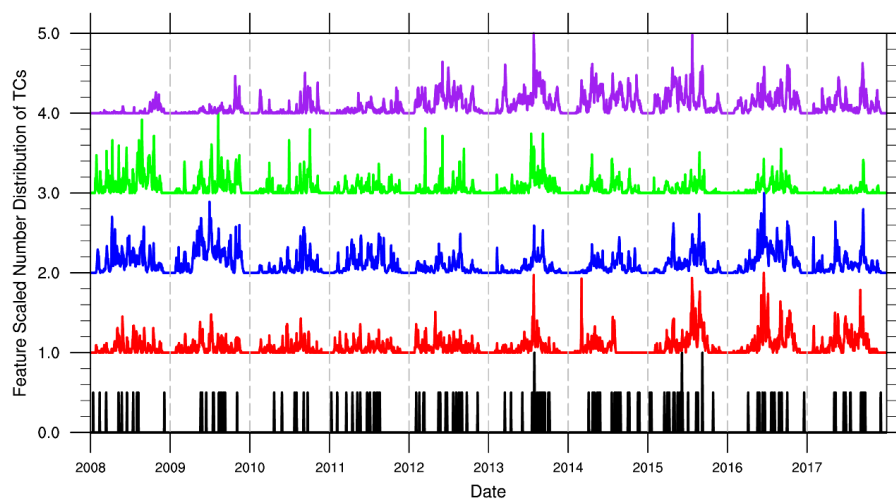
575



576

577 **Figure 2.** Ranked feature scaled track density (%) of different data sets: (a) CMA, (b) ECMWF, (c) JRA-55, (d)
578 JMA, (e) NCEP, and (f) TIGGE total. Number of TCs in the corresponding event set is stated on the top right of
579 each panel.

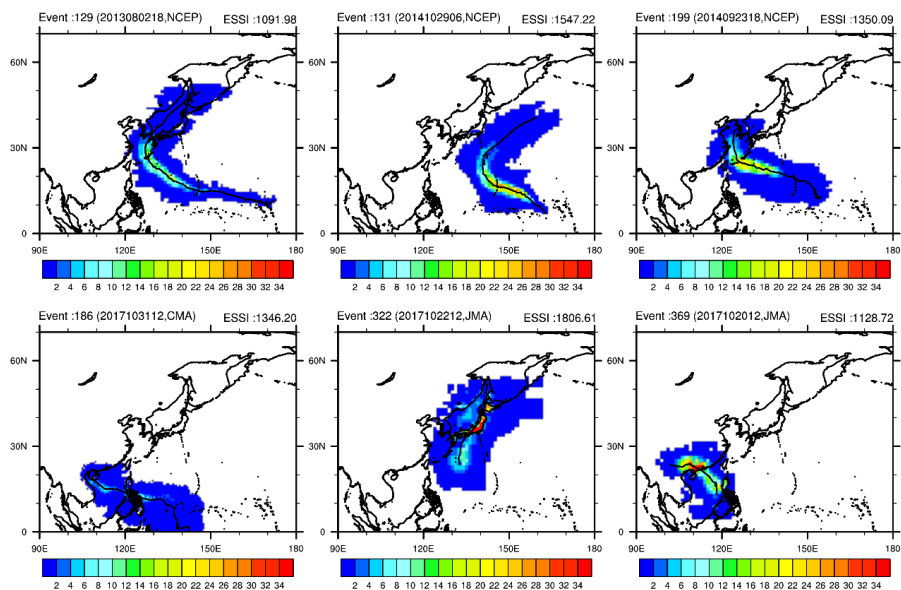
580



581

582 **Figure 3.** Feature scaled time series of number of TCs formation of TPEPS TC event set (CMA: red, ECMWF:
583 blue, JMA: green, NCEP: purple) and JRA-55 event set (black). For visual convenience, the time series of CMA,
584 ECMWF, JMA, and NCPE are shifted by 1, 2, 3, 4, respectively.

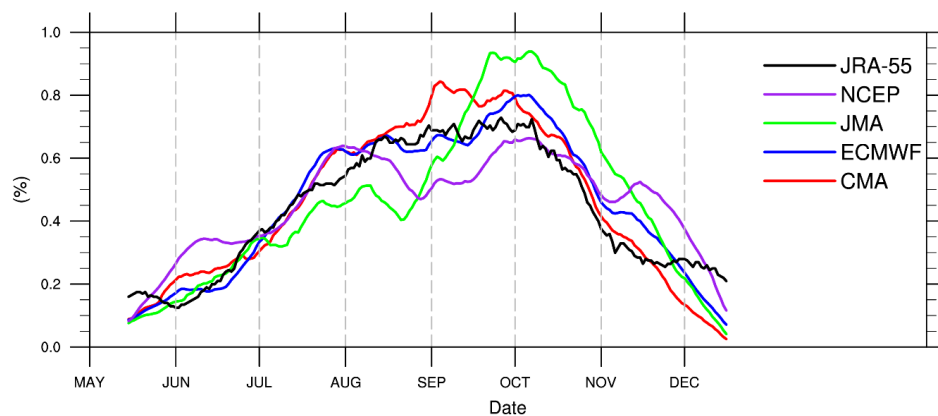
585



586

587 **Figure 4.** Some of the PEPS TC impact footprint (colour contours) and tracks (black line within the colour
588 contours) of the TPEPS TC event sets. The colour contours show the cumulative SSI of the PEPS TCs over their
589 respective lifetime at individual grid box. ESSI of each PEPS TC is shown on the top right of each panel.

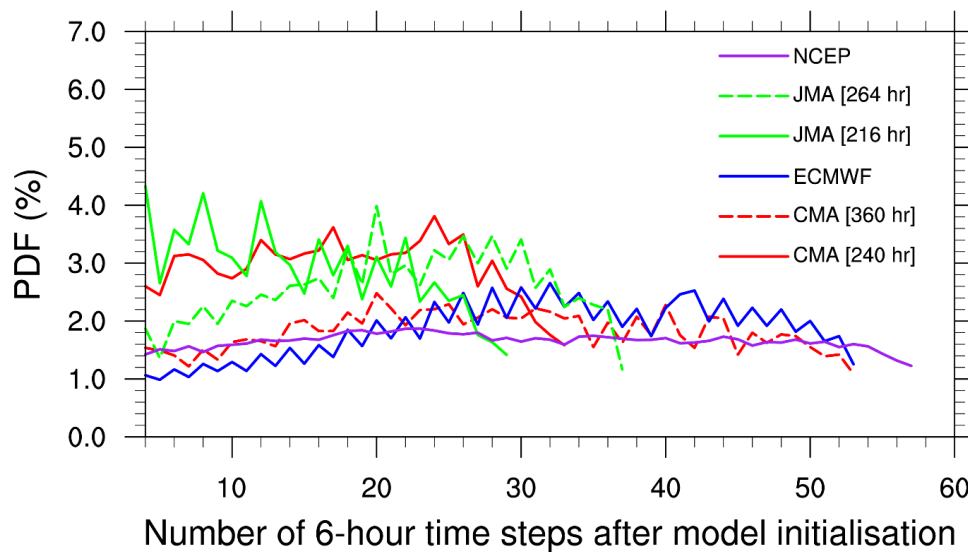
590



591

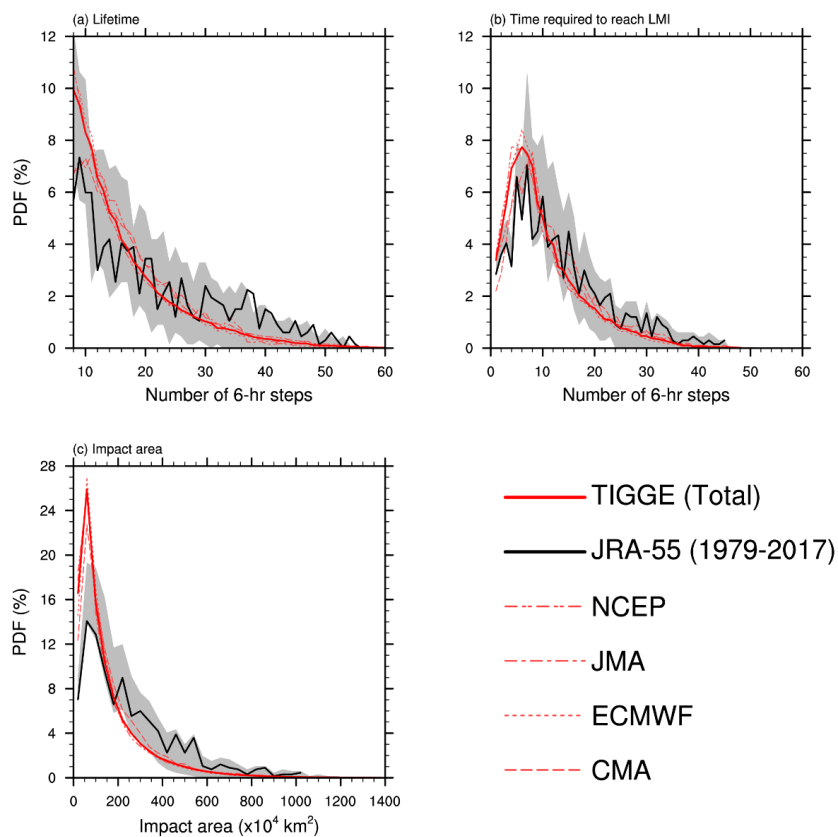
592 **Figure 5.** Climatological daily number distribution of TC for TPEPS TC event set (CMA: red, ECMWF: blue,
593 JMA: green, NCEP: purple) and JRA-55 event set (black). 30-day moving average is used in order to remove
594 high frequency signal.

595



596

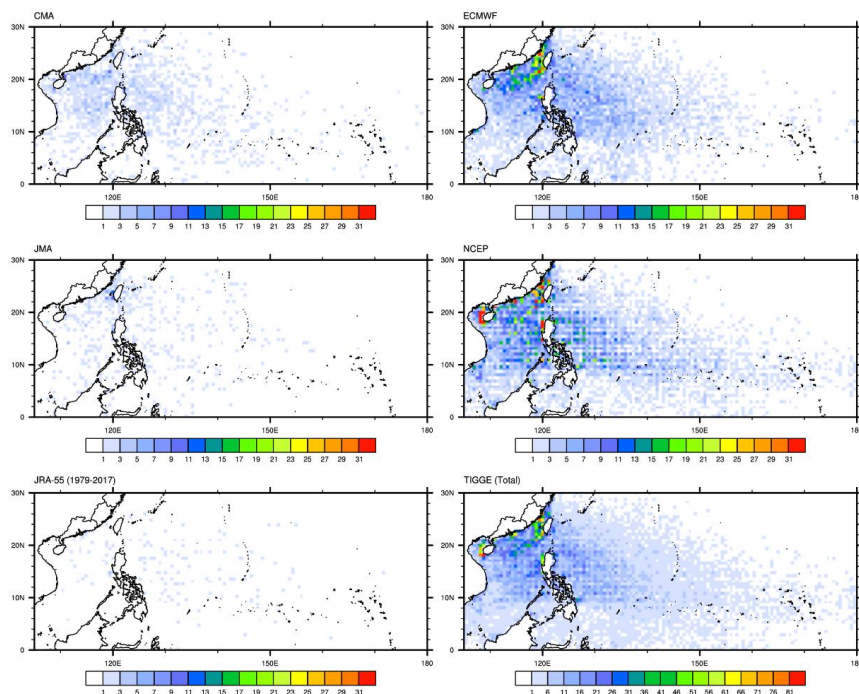
597 **Figure 6.** Temporal evolution of frequency of first storm detections of TPEPS event set (CMA: red, ECMWF:
598 blue, JMA: green, NCEP: purple).



599

600 **Figure 7.** The distribution of (a) lifetime, (b) time required to reach LMI, and (c) impact area of TCs in TPEPS
601 TC event set (red lines) and JRA-55 event set (black line). The grey area indicates the spread of the lifetime
602 distribution of JRA-55 if finite simulation windows are applied to the JRA-55 event set.

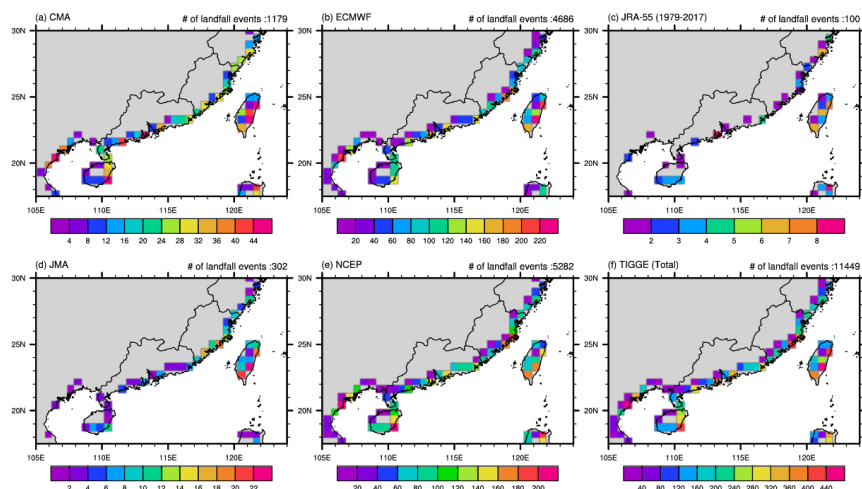
603



604

605 **Figure 8.** The spatial distribution of location of first detection of TCs (with LMI at least typhoon strength) which
606 made landfall within the domain 105-180 °E, 0-30 °N for TPEPS TC event set and JRA-55 event set.

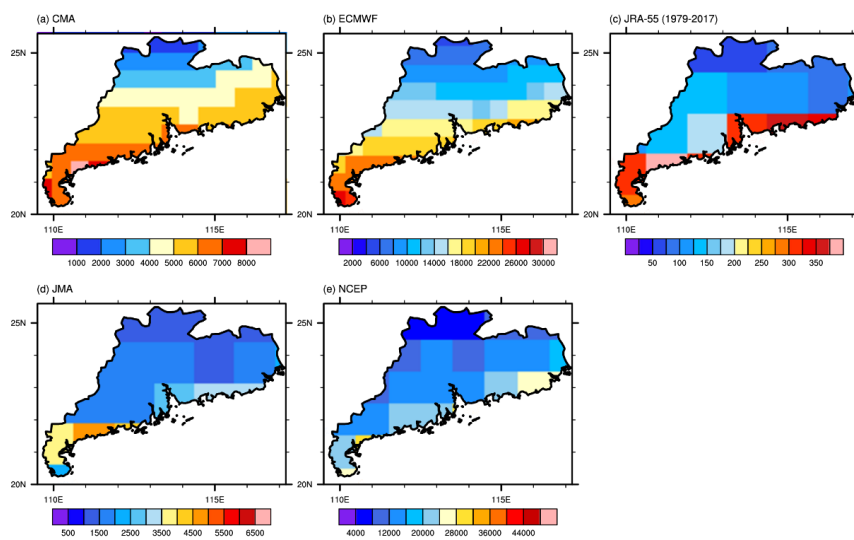
607



608

609 **Figure 9.** Spatial distribution of number of landfall events (landfall with at least typhoon strength) for TPEPS TC
610 event sets and JRA-55 event set (colours). The total number of landfall events in each panel is shown on the top
611 right of each panel.

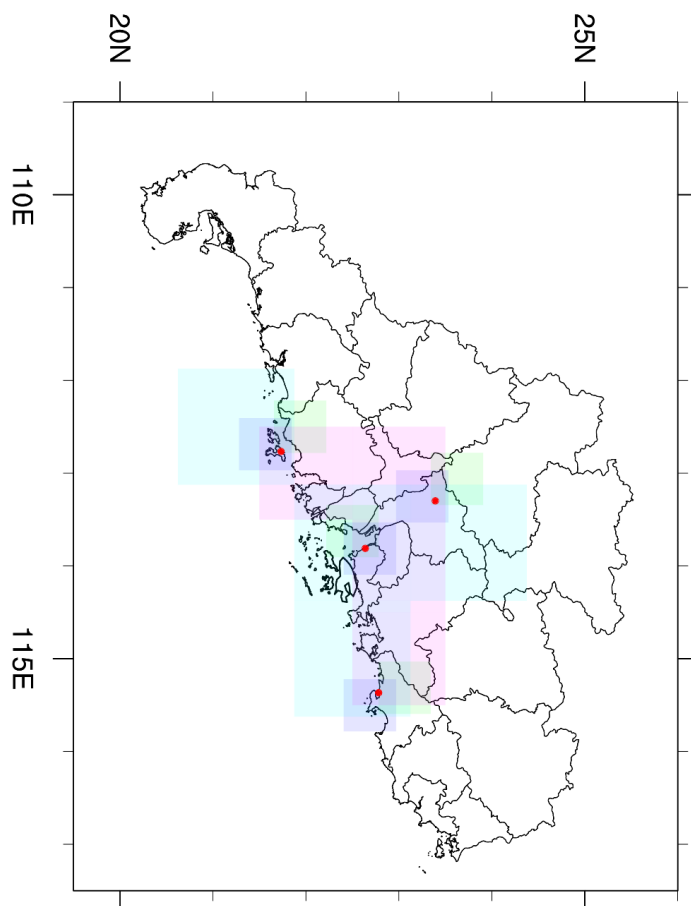
612



613

614 **Figure 10.** Number of TC-related 6-hourly data entries in each of the grid box in Guangdong Province, China,
615 for TPEPS TC event sets and JRA-55 event set.

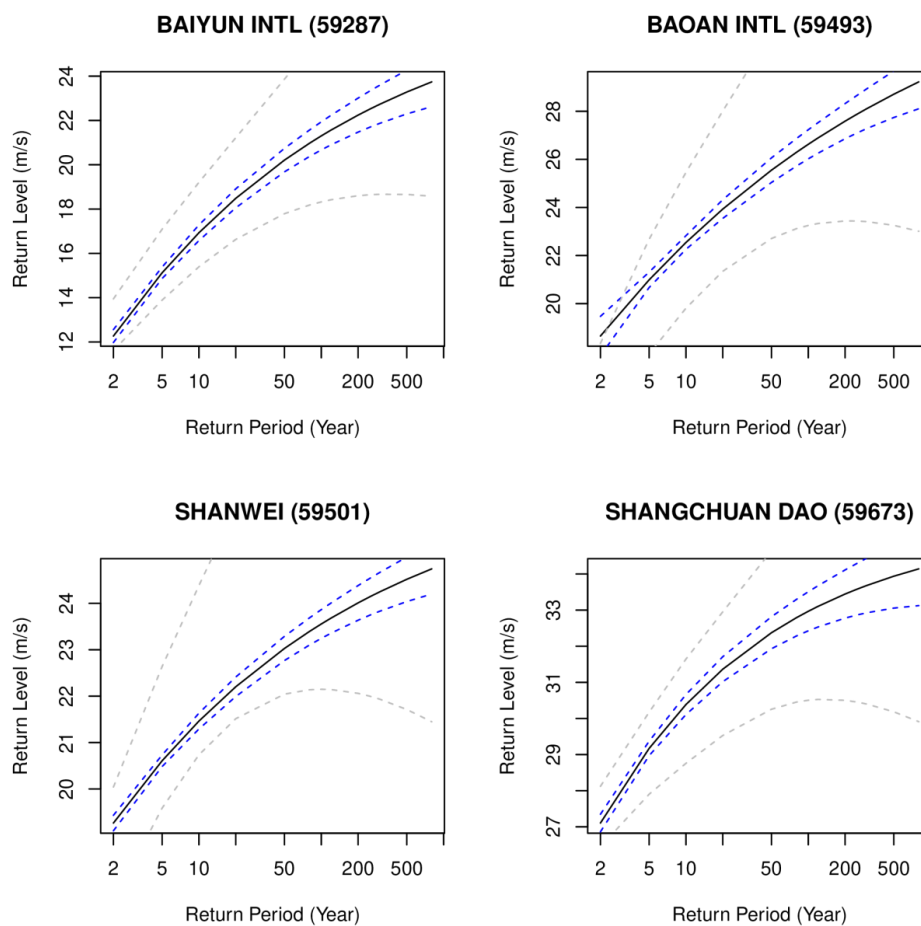
616



617

618 **Figure 11.** Locations of the selected surface observation stations (red dots) in Guangdong, China with
619 corresponding grid boxes from 4 EPS outputs: CMA (green), ECMWF (blue), JMA (cyan), and NCEP (magenta).
620 Information of prefectural boundaries is obtained from GADM version 3.6 Level 2 (available at
621 <https://gadm.org/data.html>)

622



623

624 **Figure 12.** Return period-return level plot for 4 selected surface observation stations: Baiyun International Airport,
625 Baoan International Airport, Shanwei, and Shangchuan Dao. Black lines indicate the best estimate of return period-
626 return level. Blue lines indicate the 95% confidence interval calculated using TIGGE PEPS event set. Grey lines
627 indicate the 95% confidence interval calculated using in situ observations.